Cronfa - Swansea University Open Access Repository

_____

This is an author produced version of a paper published in:
The Journal of Physical Chemistry Letters

_____

Cronfa URL for this paper:
http://cronfa.swan.ac.uk/Record/cronfa50987

_____

Paper:

_____

http://www.swansea.ac.uk/library/researchsupport/ris-support/

Measuring Energetic Disorder in Organic Semiconductors Using the Photo-Generated Charge-Separation Efficiency

Samantha Hood,[†] Nasim Zarrabi,[‡] Paul Meredith,[‡] Ivan Kassal,[*,¶] and Ardalan Armin[*,‡]

[†]*Centre for Engineered Quantum Systems and School of Mathematics and Physics, The University of Queensland, Brisbane QLD 4072, Australia*

[‡]*Department of Physics, Swansea University, Singleton Park, Swansea SA2 8PP Wales, United Kingdom*

[¶]*School of Chemistry and University of Sydney Nano Institute, University of Sydney, NSW 2006, Australia*

E-mail: i.kassal@sydney.edu.au; ardalan.armin@swansea.ac.uk

Abstract

Understanding and quantifying energetic disorder in organic semiconductors continues to attract attention because of its significant impact on the transport physics of these technologically important materials. Here, we show that the energetic disorder of organic semiconductors can be determined from the relationship between the internal quantum efficiency of charge generation and the frequency of the incident light. Our results for a number of materials suggest that energetic disorder in organic semiconductors could be larger than previously reported, and we advance ideas as to why this may be the case.

1
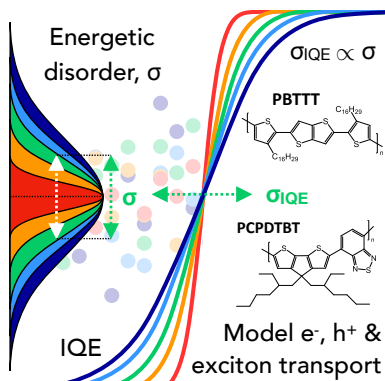
For Table of Contents Only

Organic semiconductors, and especially conjugated polymers, are energetically disordered due to conformational variation, which causes an essentially random electrostatic landscape for the charges to navigate. The energetic disorder is usually modelled as a static distribution—typically Gaussian—of the energies of the highest occupied and lowest unoccupied molecular orbitals (HOMOs and LUMOs). Energetic disorder affects organic semiconductor device performance, playing a decisive role in almost all excitonic and electronic processes, from exciton diffusion[1] and charge transport[2–6] to charge dissociation and recombination[7–10], and open circuit voltage[11,12]. Understanding and controlling disorder is thus fundamental, and its measurement remains an ongoing challenge in the field. Energetic disorder in organic semiconductors is usually measured in one of three ways, using Urbach tails in solid-state absorption spectra, via charge-transport studies, or Kelvin probe measurements of band-bending.

The Urbach tail is the exponential sub-bandgap tail formed when the optical absorption onset is broadened by energetic disorder[13,14]. The width of the tail (the Urbach energy) correlates with disorder in inorganic semiconductors such as amorphous silicon[15], and many studies have used it to also measure disorder in organic semiconductors[16–22]. However, this is known to be challenging in organic semiconductors, since they invariably lack sharp absorption onsets and have homogeneously broadened absorption features, the latter making it difficult to extract the inhomogeneous disorder. As a result of these limitations, Urbach

2

energy measurements on organic semiconductors should be understood to have substantial uncertainty, which is often not appreciated.

Disorder can also be characterised indirectly by measuring charge or exciton transport. Various transport models include energetic disorder as a fitting parameter[3,10–12,23–30]. Most commonly, carrier mobility is measured as a function of temperature and fitted to a theoretical model of thermally activated hopping. Given the relatively low electrical conductivities of these semiconductors and their inverse temperature-mobility relationship, the low-temperature measurement limit is severely restricted, often to about 200 K. As a result, it can be difficult to robustly fit temperature-dependent experimental data to theoretical models with several fit parameters over a small range of inverse temperature.

The density of tail states in organic semiconductors has been determined using Kelvin probe measurements[31,32]. This non-contact technique measures the potential difference between the probe tip and the surface of an organic film on a metallic substrate and can detect electrostatic gradients in the organic semiconductor resulting from band-bending between the organic and metallic layers. Band-bending is caused by the diffusion of charge carriers across the junction to establish thermodynamic equilibrium, with the amount of band-bending not only proportional to the energy difference between the materials but also to the width of the density of states (DOS) near the surface of the film[33]. Alongside this technique, Kelvin probe force microscopy can also be used to measure the tails of the DOS with a field-effect transistor configuration[34,35]. As emphasised in a recent review on the measurement of energetic disorder in organic semiconductors by Karki et al.[32], the band-bending technique is mainly sensitive to the tails in the DOS and is relevant to the surface of the semiconductor.

Most device-level mobility measurements probe thermalised carriers, which occupy the tails of the DOS. This can lead to serious inaccuracies if the tails deviate even slightly from perfect Gaussian tails, as is actually the case if the disorder is caused by randomly oriented electric dipoles[36]. These inaccuracies are compounded if the resulting disorder measurements are extrapolated to model effects like charge separation, which often depend on the full DOS,

3

rather than just its tails.

Here, we show that energetic disorder in neat organic semiconductors can be determined by measuring the internal quantum efficiency (IQE) of photo-excited charge separation as a function of excitation wavelength. Using kinetic Monte Carlo (kMC) simulations, we demonstrate that energetic disorder determines the width of the IQE increase, providing a simple way to determine the energetic disorder in neat organic semiconductors.

Our approach has three advantages over existing methods. First, unlike the Urbach tail analysis, the method is not affected by homogeneous disorder, making the spectral fitting unambiguous. Second, the measurement can be carried out at a single temperature, unlike the transport methodology. Third, the method is sensitive to the entire DOS, rather than just the tails, making the resulting disorder values suitable for modelling processes such as charge generation.

We use our technique to measure disorder in eight organic semiconductors, showing them to be generally more disordered than previously reported.

Device Fabrication and Characterisation

Pre-patterned glass substrates coated with indium tin oxide (Kintec) were cleaned using Alconax (detergent) solution and soft, lint-free swabs prior to sequential sonication with deionised water, acetone, and 2-propanol for 10 min each. Each substrate was $2.5\,\mathrm{cm} \times 2.5\,\mathrm{cm}$ in size and had six pixels with device area of $0.2\,\mathrm{cm}^2$. A $(25 \pm 5)\,\mathrm{nm}$ layer of poly(3,4-ethylenedioxythiophene):poly(styrenesulfonate) (PEDOT:PSS, from Heraeus) was then spin-coated at 5000 rpm for 60 s. The PEDOT:PSS layer was annealed for 10 min at 170 °C. Eight single-component organic semiconductor active layers (full names and structures are in fig. S1 in the Supporting Information) were spin-coated from solutions. The solvent in which each material was dissolved, solution concentration, and speed of the spin coater were as follows: **P3HT** (Merck Chemical, $\overline{M}_\mathrm{w} = 72\,\mathrm{kDa}$) dissolved in chloroform (CF), $10\,\mathrm{mg/ml}$, 2500 rpm; **PCDTBT** (SJPC Canada, $\overline{M}_\mathrm{w} = 122.2\,\mathrm{kDa}$, PDI = 5.4), dissolved in 1,2-

dichlorobenzene (DCB), 10 mg/ml, 1000 rpm; **PTB7** (1-Materials, $\overline{M}_\text{w} = 97.5$ kDa, PDI $=$ 2.1), dissolved in DCB, 20 mg/ml, 1000 rpm; **PCPDTBT** (Lumtec, $\overline{M}_\text{w} = 7-20$ kDa), dissolved in chlorobenzene (CB), 10 mg/ml, 1000 rpm; **DPP-DTT** (synthesised as previously described[37], $\overline{M}_\text{w} = 350$ kDa, PDI=2.8), dissolved in CF, 10 mg/ml, 1500 rpm; **MEH-PPV** (Sigma-Aldrich, $\overline{M}_\text{m} = 40-70$ kDa), dissolved in DCB, 5 mg/ml, 1000 rpm, **Super yellow** (PDY-132, Merck), dissolved in toluene, 7 mg/ml, 3000 rpm; and **PBTTT** (C14, Merck, $\overline{M}_\text{w} > 50$ kDa), dissolved in CB and heated to 120 °C, 6 mg/ml 1500 rpm. Finally, 70 nm of aluminium (the cathode) was evaporated under 10^{-6} mbar vacuum on the active layers with an evaporation mask (0.2 cm^2 for each device). The active-layer deposition processes were entirely performed under a nitrogen atmosphere in a glovebox within a class-1000 clean room.

To characterise the devices, the external quantum efficiency (EQE) and reflection spectra were measured (see Figs. S2 and S3 in the Supporting Information) with a QEX7 setup from PV Measurement Inc., using an integrating sphere and calibrated photodiode without light bias. The measurements were performed at 120 Hz and an electrical bandwidth of approximately 1 Hz. The IQE spectra were determined using the methodology described previously[38] and in the supporting information (fig. S4). The method is based upon measuring the reflectivity of the cell and accounting for parasitic absorptions. This methodology directly measures the probability that a photo-excitation will yield extracted charges as opposed to recombining in the active layer or at the electrodes.

Simulation Details

We model the charge generation in a single-component organic semiconductor using kMC simulations on a cubic lattice of $30 \times 30 \times 30$ sites, with periodic boundary conditions and lattice constant a. Each lattice site represents a molecule and has two energies associated with it, one for the HOMO (E_HOMO^i) and one for the LUMO (E_LUMO^i). Each of these energies
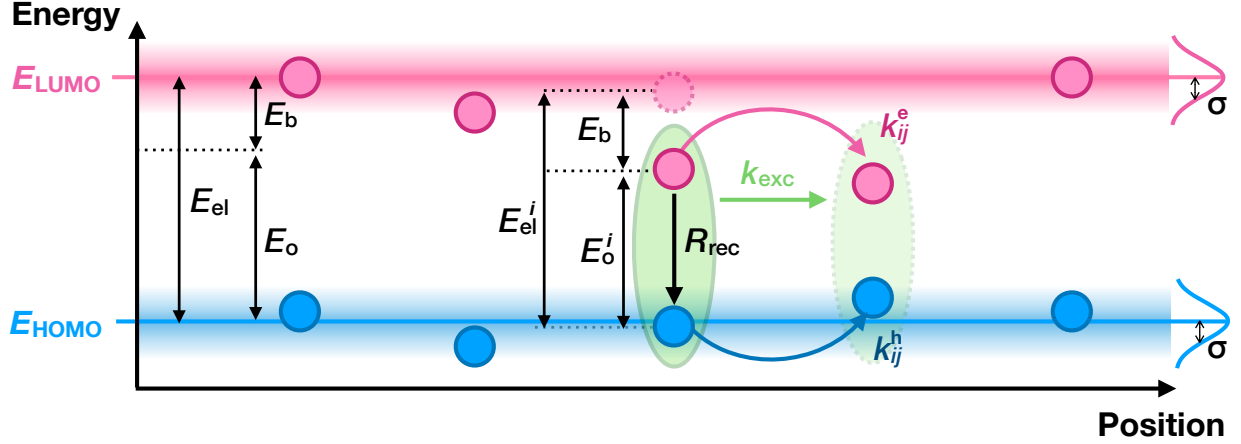
Figure 1: Energies and rates relevant to an organic semiconductor photo-junction and useful to understand our simulation construct and the mode of device operation. $E_{\mathrm{el}} = E_{\mathrm{LUMO}} - E_{\mathrm{HOMO}}$ is the average electronic gap, E_{b} is the exciton binding energy (assumed constant) and $E_{\mathrm{o}} = E_{\mathrm{el}} - E_{\mathrm{b}}$ is the average optical gap. Both HOMO and LUMO levels are broadened by including Gaussian energetic disorder with standard deviation σ, which makes the electronic and optical gaps vary from site to site (denoted E_{el}^i and E_{o}^i at site i). An exciton, shown at site i, can dissociate by a charge hopping event to an adjacent site at rate k_e^{ij} or k_h^{ij}, hop to a neighbouring site at rate k_{exc}, or recombine at rate R_{rec}.

contains energetic disorder, drawn independently from a Gaussian DOS of width σ (fig. 1),

$$g(E_{\mathrm{HOMO}}^i) = \frac{1}{\sqrt{2\pi\sigma^2}} \exp\left(-\frac{(E_{\mathrm{HOMO}}^i - E_{\mathrm{HOMO}})^2}{2\sigma^2}\right), \tag{1}$$

and analogously for E_{LUMO}^i. The electronic gap of site i is $E_{\mathrm{el}}^i = E_{\mathrm{LUMO}}^i - E_{\mathrm{HOMO}}^i$ and its optical gap is $E_{\mathrm{o}}^i = E_{\mathrm{el}}^i - E_{\mathrm{b}}$, where the exciton binding energy E_{b} is assumed to be constant at all sites.

We assume that a site can absorb a photon of energy E_{p} if $E_{\mathrm{p}} > E_{\mathrm{o}}^i$. To initialise a simulation under illumination with photons of energy E_{p}, one of the sites where $E_{\mathrm{o}}^i < E_{\mathrm{p}}$ is randomly selected to be where the exciton forms. Any excess energy above E_{o}^i is assumed lost before the next simulation step, i.e., we do not consider vibrationally or electronically hot excitons, assuming that excitons will thermalise much faster than they dissociate. After the initialisation, the four elementary processes that can happen at each step of the simulation are illustrated in fig. 1: either the electron or the hole can hop independently to a neighbouring

Table 1: Parameters for the kinetic Monte-Carlo simulations and their effect on the width σ_{IQE} and position E_{IQE} of the predicted IQE. In each case, the sensitivity is the slope of the linear regression as a function of the parameter. σ is the electronic disorder, R_{rec} the recombination rate, V_{ij} the nearest-neighbour electronic coupling, E_{el} the mean electronic gap, E_{b} the exciton binding energy, λ the reorganisation energy, a the lattice spacing, d_{l} the dissociation length, and $k_{\text{exc},0}$ the exciton hopping prefactor. Most importantly, the IQE width σ_{IQE} is almost entirely determined by the microscopic energetic disorder σ.

Parameter	Baseline value	Range	Sensitivity of σ_{IQE}	Sensitivity of E_{IQE}
σ	$200\,\text{meV}$	$100-300\,\text{meV}$	2.26 ± 0.10	n/a; minimum at $250\,\text{meV}$
R_{rec}	$10^{10}\,\text{s}^{-1}$	$10^{9}-10^{11}\,\text{s}^{-1}$	$(1 \pm 2) \times 10^{-10}\,\text{meV}\,\text{s}^{-1}$	$(2.4 \pm 6.4) \times 10^{-9}\,\text{meV}\,\text{s}^{-1}$
V_{ij}	$1.6\,\text{meV}$	$1.6-16\,\text{meV}$	-3.7 ± 4.4	-8.6 ± 4.5
E_{el}	$3.6\,\text{eV}$	$3.3-3.9\,\text{eV}$	n/a; maximum at $3.6\,\text{eV}$	0.99 ± 0.15
E_{b}	$0.7\,\text{eV}$	$0.5-0.9\,\text{eV}$	0.1 ± 0.1	0.15 ± 0.35
λ	$200\,\text{meV}$	$100-300\,\text{meV}$	0.12 ± 0.18	0.28 ± 0.02
a	$1\,\text{nm}$	$1-2\,\text{nm}$	$(80 \pm 10)\,\text{meV}\,\text{nm}^{-1}$	$(140 \pm 100)\,\text{meV}\,\text{nm}^{-1}$
d_{l}	$5\,\text{nm}$	$3-7\,\text{nm}$	n/a; maximum at $5\,\text{nm}$	$(20 \pm 10)\,\text{meV}\,\text{nm}^{-1}$
$k_{\text{exc},0}$	$10^{11}\,\text{s}^{-1}$	$10^{10}-10^{12}\,\text{s}^{-1}$	$(4.5 \pm 13.0) \times 10^{-11}\,\text{meV}\,\text{s}^{-1}$	$(3 \pm 4) \times 10^{-10}\,\text{meV}\,\text{s}^{-1}$

site, the exciton as a whole can hop to a neighbouring site, or the exciton can recombine.

Electron hopping from current site i to a neighbouring site j occurs at the Marcus rate[39]

$$k_e^{ij} = \frac{2\pi}{\hbar} \frac{|V_{ij}|^2}{\sqrt{4\pi\lambda k_{\text{B}}T}} \exp\left(\frac{-(\Delta E_{\text{LUMO}}^{ij} + \Delta U^{ij} + \lambda)^2}{4\lambda k_{\text{B}}T}\right), \tag{2}$$

where V_{ij} is the electronic coupling between the sites, $\Delta E_{\text{LUMO}}^{ij} = E_{\text{LUMO}}^{j} - E_{\text{LUMO}}^{i}$, λ is the reorganisation energy, and ΔU^{ij} is the difference in the Coulomb potential between the two charge configurations. In particular, $\Delta U^{ij} = U(r^j) - U(r^i)$, where r^i is the distance between site i and the location of the hole (which does not move during electron hops), and $U(r) = e^2/4\pi\epsilon_r\epsilon_0 r$, where e is the elementary charge, ϵ_r is the dielectric constant, and ϵ_0 is the vacuum permittivity. If the charges are on the same molecule ($r = 0$, i.e., the charges form an exciton), the Coulomb interaction $U(r)$ is replaced by the exciton binding energy E_{b}.

Hole hopping is analogous to electron hopping, except that E_{LUMO}^{ij} is replaced with E_{HOMO}^{ij} in eq. 2.

Exciton hopping is a possible process if, at a particular step in the simulation, the elec-

tron and the hole are on the same site. Exciton transfer is most commonly described by Förster theory, but to reduce the number of free parameters we modelled it using the Miller-Abrahams expression[40],

$$k_{\text{exc}}^{ij} = k_{\text{exc},0} \begin{cases} e^{-\left(E_{\text{exc}}^{j} - E_{\text{exc}}^{i}\right)/k_{\text{B}}T} & \text{if } E_{\text{exc}}^{j} > E_{\text{exc}}^{i} \\ 1 & \text{if } E_{\text{exc}}^{j} < E_{\text{exc}}^{i}, \end{cases} \quad (3)$$

where $k_{\text{exc},0}$ is the (constant) exciton hopping attempt frequency and $E_{\text{exc}}^{i} = E_{\text{LUMO}}^{i} - E_{\text{HOMO}}^{i} - E_{\text{b}}$.

The last elementary process, exciton recombination, occurs at constant rate R_{rec} if both charges are on the same site.

The kMC simulation tracks the positions of the electron and the hole as they undergo the elementary processes described above. At each step of the simulation, the rate of each possible elementary process is calculated, and the mth process, occurring at rate k_m, is allocated a time $t_m = -\ln(\rho_m)/k_m$, where ρ_m is a random number uniformly distributed between 0 and 1. The process with the smallest t_m is then selected to occur. This process is repeated until either the charges have recombined, become separated by more than a cut-off distance d_l, or have done 2000 hops (in which case they are assumed to have recombined). The IQE is calculated as the fraction of trajectories in which the charges separate instead of recombining. For a given realisation of energetic disorder, an exciton is created and 50 trajectories are averaged over to determine the average IQE for this realisation of disorder. The disordered landscape is also realised 5000 times for each value of σ to determine the average IQE.

Parameters that were held fixed in all simulations were $T = 300\,\text{K}$ and $\epsilon_r = 3.5$. For each of the other parameters a baseline value, shown in table 1, was chosen based on literature values; e.g., $\lambda = 200\,\text{meV}$[22,41], $V_{ij} = 1.6\,\text{meV}$ (for nearest neighbours only, so that the prefactor of the exponential function is $10^{11}\,\text{s}^{-1}$[10]), and $E_{\text{b}} = 700\,\text{meV}$[16]. In addition, a one-

factor-at-a-time (OFAT) sensitivity analysis was carried out for each parameter, by scanning its value over the range also specified in table 1. A total of 2500 energetic landscapes were averaged over for each parameter value. Plots of the IQE results from the parameter sweeps are in the Supporting Information in fig. S5.

Simulation Results

Fig. 2a shows the predicted spectral dependence of the IQE of charge generation in a neat material. Higher values of the photon energy E_p result in higher IQEs, showing that excitons created higher in the disorder distribution are more likely to separate into charges. A more energetic photon can excite sites that, because of energetic disorder, have either high-lying LUMOs or low-lying HOMOs. That excitation makes it likely that one of the neighbouring sites has either a lower-lying LUMO or a higher-lying HOMO, making it energetically favourable for the electron or hole, respectively, to hop onto the neighbour. This disorder-driven initial separation reduces the likelihood of geminate recombination because the charges are less likely to return to the first site, which would requires them to move uphill in energy. Once they have taken one hop away from each other, the Coulomb attraction between charges is lowered, facilitating further charge separation.

The simulation results can be fitted very well using the error function

$$\text{IQE}(E_p) = \frac{\text{IQE}_{max}}{2}\left(\text{erf}\left(\frac{E_p - E_{IQE}}{\sigma_{IQE}}\right) + 1\right) + \text{IQE}_0, \tag{4}$$

where the shape of the curve is governed by its midpoint E_{IQE} and width σ_{IQE}, and its height and vertical offset by IQE_{max} and IQE_0, as shown in fig. 2a. In simulations, $\text{IQE}_0 = 0$, but we include it as a fitting parameter to allow the subtraction of experimental baselines, such as exciton quenching by impurity states or excitons quenching at electrodes.

The form of eq. 4 can be understood using a simplified model. The IQE can be calculated exactly if downhill electron hopping is assumed to be much faster than recombination,
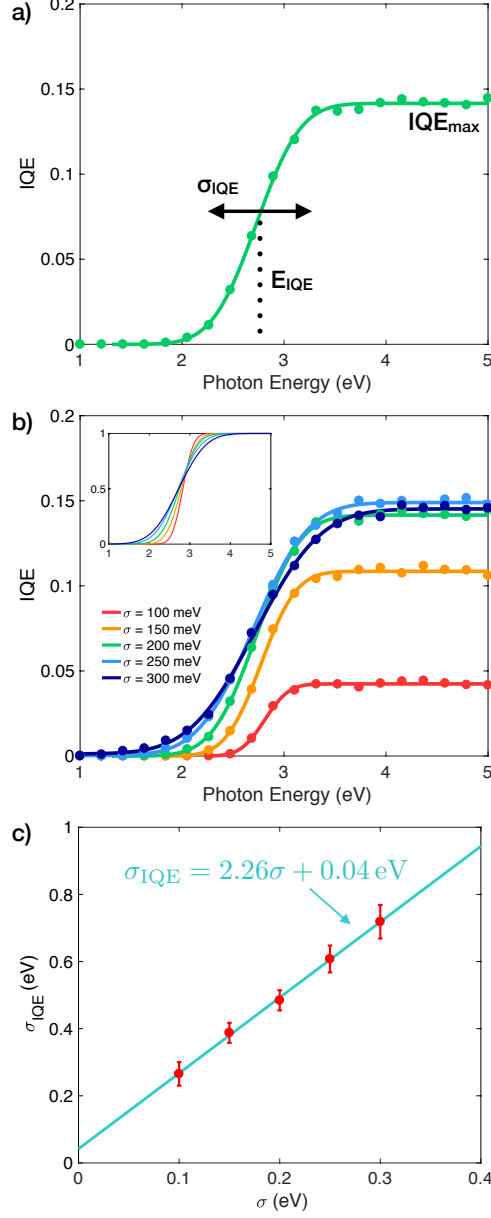
9

Figure 2: Simulation results. **a)** The predicted energy dependence of the internal quantum efficiency (IQE) when the simulation parameters take on the baseline values in table 1. The solid line is the fit to the error function in eq. 4, which defines its width σ_{IQE}, position E_{IQE}, and maximum value IQE_{max}. **b)** Changing the microscopic energetic disorder σ (while keeping other parameters fixed) changes σ_{IQE}, E_{IQE}, and IQE_{max}. The inset normalised plots highlight how σ_{IQE} depends on σ. **c)** Sensitivity analysis. σ_{IQE} is close to proportional to σ, with slope (sensitivity) 2.26 ± 0.10. Each data point is obtained from the fits in panel b.

while the remaining rates—uphill electron hopping, hole hopping, and exciton hopping—are neglected. Assuming that each site has only one neighbour, the IQE becomes equal to the

probability that the initial LUMO (E_{LUMO}^i) lies above the LUMO of its neighbour (E_{LUMO}^f). This has to be conditioned on the initial site being able to absorb the incoming photon, $E_{\mathrm{exc}}^i < E_{\mathrm{p}}$, giving $\mathrm{IQE}(E_{\mathrm{p}}) = \mathrm{Prob}(E_{\mathrm{LUMO}}^i > E_{\mathrm{LUMO}}^f \,|\, E_{\mathrm{LUMO}}^i - E_{\mathrm{HOMO}}^i - E_{\mathrm{b}} < E_{\mathrm{p}})$, where E_{LUMO}^i, E_{HOMO}^i, and E_{LUMO}^f are independent, normally distributed random variables, as described above. Evaluating this conditional probability gives

$$\mathrm{IQE}(E_{\mathrm{p}}) = \frac{1}{4}\left(\mathrm{erf}\left(\frac{E_{\mathrm{p}} - (E_{\mathrm{LUMO}} - E_{\mathrm{HOMO}} - E_{\mathrm{b}})}{2\sigma}\right) + 1\right). \tag{5}$$

Comparing eq. 5 with eq. 4 shows that the simple model suggests $\sigma_{\mathrm{IQE}} = 2\sigma$, $E_{\mathrm{IQE}} = E_{\mathrm{LUMO}} - E_{\mathrm{HOMO}} - E_{\mathrm{b}}$, and $\mathrm{IQE}_{max} = 1/2$. Although the model omits many features of the full simulation—including multiple nearest neighbours, exciton and hole hopping, uphill electron hops, and recombination after the initial hop—it does capture the important prediction that σ_{IQE} is around 2σ. This is both larger than might be expected, giving a very broad IQE, and, crucially, independent of the energy levels.

We used sensitivity analysis to determine the robustness of the model in eq. 4 for representing simulation data. OFAT sensitivity analysis tracks changes in outputs (E_{IQE} and σ_{IQE}) as each of the input parameters is varied independently with respect to a baseline value. Although it does not explore the full parameter space (which is too large here), it does offer valuable insights about which parameters contribute most to which outputs.

Fig. 2b shows how the IQE rise changes as input parameter σ is varied, revealing that it affects both E_{IQE} and σ_{IQE} (as well as $\mathrm{IQE}_{\mathrm{max}}$). The linear relationship between σ_{IQE} and σ is shown in fig. 2c, and the sensitivity of the σ_{IQE} on σ is the slope of the linear regression. The plots of the IQE rise as a function of changes in each of the other microscopic parameters are shown in the Supporting Information in fig. S5. The results are summarised in table 1, which shows the sensitivity of σ_{IQE} and E_{IQE} to each of the parameters. These results are also presented graphically in Figs. S6 and S7 in the Supporting Information.

The dependence of E_{IQE} on the model parameters is complicated. It is most sensitive

to E_{el}, as expected: widening the electronic gap means more energy is needed to create excitons in the first place. However, E_{IQE} also depends appreciably on most of the other parameters, including σ, R_{rec}, V, and $k_{exc,0}$. Consequently, a measurement of E_{IQE} is not a useful experimental proxy of an underlying microscopic parameter.

By contrast, σ_{IQE} is almost entirely determined by σ. The sensitivity of σ_{IQE} on the other parameters is either much smaller than it is on σ or is statistically indistinguishable from zero (or both). Over the realistic parameter ranges in table 1, changing σ changes σ_{IQE} by 450 meV; the second largest change is due to the lattice spacing a, but amounts to only 80 meV.

Therefore, σ_{IQE} is a robust experimental proxy for σ. After neglecting the insignificant parameters, we arrive at the linear relationship

$$\sigma_{IQE} = (2.26 \pm 0.10)\sigma + (40 \pm 20)\, \text{meV}, \tag{6}$$

which is not too far from the crude prediction $\sigma_{IQE} = 2\sigma$.

For the sake of completeness, we also carried out kMC simulations of charge separation in which the exciton was not allowed to diffuse before charge separation. These results are reported in the Supporting Information (table S1 and fig. S8) and show that there is a substantial difference between IQEs calculated with and without exciton diffusion, confirming the need to include exciton diffusion if realistic results are to be obtained. We also investigated (Supporting Information figs. S9-S11) the effect of an applied electric field on the IQE both experimentally and within simulations. We found that the width (σ_{IQE}) and the position (E_{IQE}) of the IQE were not significantly affected by typical values of the electric field.

Measuring Energetic Disorder in Semiconducting Polymers

We applied our theory to determine the energetic disorder of several neat semiconducting polymers. Fig. 3 shows the measured spectral dependence of their IQEs, along with the clear agreement with the predicted error-function shape of eq. 4. We eliminated the need to measure absolute IQEs by normalising the plateaued maximum in the experimental data for each material. This allowed us to characterise the shape of the IQE curves with just the regression parameters σ_{IQE} and E_{IQE}, which are also shown in fig. 3. The value of IQE_0 is non–zero for some materials; we attribute this to either impurities acting as exciton quenchers or to excitons reaching and dissociating at an electrode. In some cases, IQE_0 appears considerable because of the normalisation (for example MEH-PPV).

We estimated the energetic disorder σ from σ_{IQE} using eq. 6, with results also shown in fig. 3. Our sensitivity analysis allowed us to estimate the uncertainty of the resulting values, which is usually not reported in the literature. In most cases, the uncertainty is small, reflecting the robustness of our approach. The larger uncertainties obtained for MEHPPV, PB-TTT and Super Yellow were caused by these materials' high E_{IQE}, which prevented us from gathering sufficient data at higher photon energies, reducing the quality of the fit.

Our values of σ, ranging from $150\,\text{meV}$ to $205\,\text{meV}$, are generally higher than the $100\,\text{meV}$ that has been used as the rule of thumb for energetic disorder in organic semiconductors[3,6,7,42,43]. Because an energetic disorder of $100\,\text{meV}$ applies to the inhomogeneous width of the S_1 band in vapour-deposited tetracene[42], it is likely that the materials measured here, with their considerably greater conformational variation, would be significantly more disordered.

Indeed, most previous estimates of energetic disorder for the polymers measured here are lower than ours. Energetic disorder in PCPDTBT and PTB7 has been estimated (by measuring Urbach energies) to be $75\,\text{meV}$ and $50\,\text{meV}$, respectively[22]. For P3HT, temperature-dependent mobility measurements were reproduced using simulations that used energetic disorder of $70\,\text{meV}$[44], a value consistent with estimates by[45] using the same technique. For
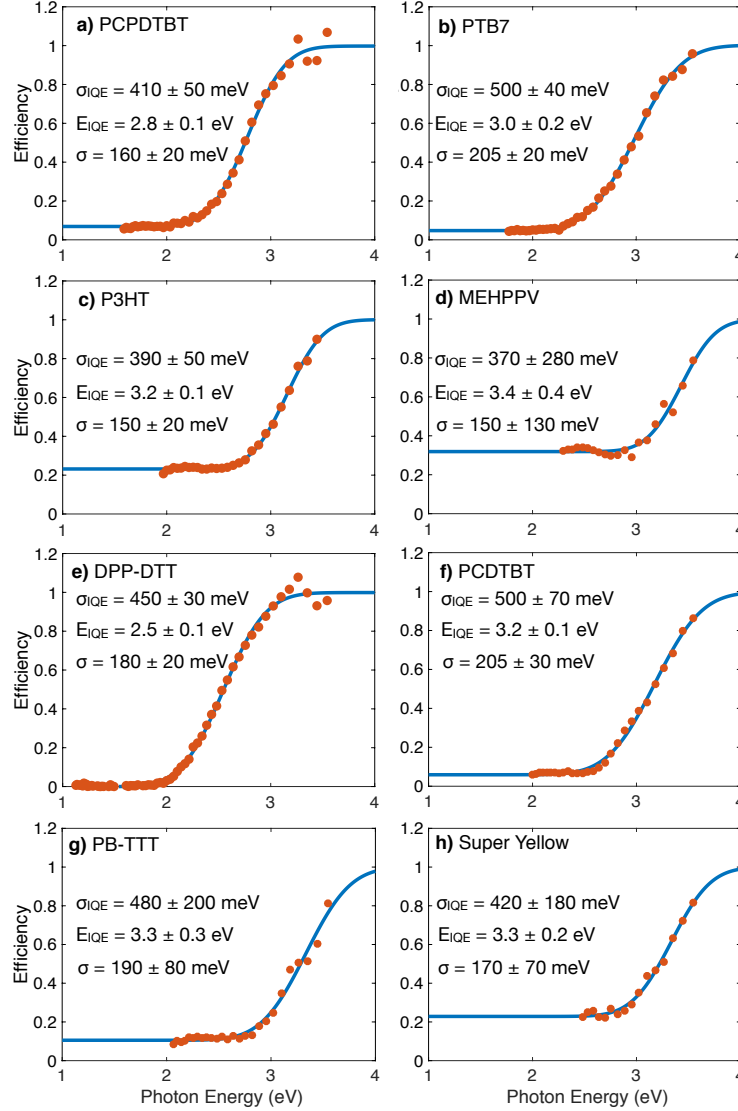
Figure 3: Experimental results. The red points are experimental IQEs and the blue curves are fits to the error function eq. 4, which determines the position E_{IQE} and width σ_{IQE}. The data was scaled so that the fit saturates at 1. σ is the microscopic energetic disorder calculated from σ_{IQE} using eq. 6.

MEH-PPV, σ was estimated to be 105 meV via Monte Carlo charge transport simulations of exciton lifetimes [29]. From time-of-flight measurements, the disorder in MEH-PPV was found to be 63 meV or 92 meV (depending on the solvent) [46]. For PCDTBT, a value of 110 meV was reported for the energetic disorder of the HOMO level of a PCDTBT:PC$_{61}$BM blend using kMC simulations of thermalisation with Gaussian disorder [47]. There is a large uncertainty associated with energetic disorder for materials with variable degree of crystallinity.

For example, the Urbach energy from absorption measurements gave an energetic disorder of the HOMO in crystalline PB-TTT to be $30\,\mathrm{meV}$ but $108\,\mathrm{meV}$ for amorphous PB-TTT[19].

Some studies, however, do predict energetic disorders significantly above $100\,\mathrm{meV}$. Super Yellow has been estimated to have $140\,\mathrm{meV}$ of energetic disorder via Monte Carlo charge-transport simulations[29]. Measurements of recombination of photogenerated charge carriers in a disordered polymer-fullerene blend gave an energetic disorder of $\sigma = 150\,\mathrm{meV}$[48]. In their recent paper, Karki et al. used the Kelvin probe technique to measure $\sigma = (130 \pm 25)\,\mathrm{meV}$ for MEH-PPV (and $\sigma = (70 \pm 15)\,\mathrm{meV}$ for PTB7), with transport measurements giving them similar values for each material (assuming a Gaussian DOS). Kelvin probe techniques measure the tails of the DOS, and J-V measurements are also likely to sample the tails as the charges thermalise during transport, so it is possible the entire DOS is broader than the range they sample. Measurements of disorder of interfacial charge-transfer states found $\sigma_{\mathrm{CT}} = 70 - 100\,\mathrm{meV}$[49]; it is likely that the energetic disorder experienced by free charges is greater than this value because charges are more sensitive to random electric fields.

The larger values obtained by our IQE technique could be more representative of the actual energetic disorder in the eight polymers studied than those obtained by other methods. Our technique samples the entire density of states, because the increase of the IQE with excitation frequency reflects the accessibility of states at higher energies. By contrast, transport measurements tend to sample only the thermally accessible states (in the tails of the DOS), leading to an underestimation of the energetic disorder that is actually present. Therefore, our technique is complementary to previous methods as it provides a measure of the disorder relevant to charge separation as opposed to charge transport.

One limitation of the current technique is the experimental difficulty in achieving high enough photon energies above the optical gap for large gap materials. Having these higher photon energy measurements allows for a more accurate fitting of our IQE model. This limitation leads to uncertainty in the extracted parameters such as in the case of MEH-PPV, PB-TTT and Super Yellow. For these large gap materials, the EQE needs to be

measured deeper in the UV which is experimentally difficult. Therefore, our technique is currently best applied to narrow and mid-gap systems amenable to EQE measurements over a wider range of photon energies.

Our model could be refined by relaxing some of its assumptions.

First, correlations could be added to the disorder. In particular, HOMO and LUMO energies are known to be correlated, resulting in excitonic disorder that is usually lower than if the electronic energies were uncorrelated[3]. In addition, the energy levels of nearby molecules are potentially also correlated. Including spatial correlation would smooth the electronic landscape, meaning that even larger values of σ would be needed to reproduce the IQE curves we observed. Additionally, future models could include asymmetric disorder between the HOMO and LUMO levels to replicate unipolar transport.

Second, our model includes only static energetic (diagonal) disorder, which is thought to be the dominant contribution. It could be extended to include either dynamic disorder or disorder in intermolecular couplings (off-diagonal disorder). The contributions of static and dynamic disorder were distinguished for a range of fullerenes[50], with the static disorder being about twice as large as the dynamic disorder. Our σ reflects the instantaneous sum of static and dynamic disorder, which form the energetic landscape seen by the light being absorbed. If these contributions were separated, the static value would be somewhat smaller than the value we report.

Third, additional structure, whether electronic or vibrational or both, could be added to each site. However, because of Kasha's rule, we do not expect that this change would significantly affect our results. Even if higher-lying electronic or vibrational states were excited, we expect that, in most materials, the exciton would relax to the lowest vibrational state of S_1 much faster than subsequent exciton or charge hopping.

We have shown that the width of the spectral increase of the IQE in a neat organic semiconductor depends almost entirely on the material's energetic disorder. Therefore, it forms an independent means for estimating the total energetic disorder, a quantity for which

no simple analysis techniques are available. Unlike measurements of Urbach energies, our approach does not require the difficult decoupling of homogeneous and inhomogeneous broadening, and, unlike temperature-dependent transport measurements, it can be carried out for a particular morphology at a particular temperature. Most importantly, our technique samples the entire DOS, and not just the tails states accessible via these previous techniques, making it particularly useful in the study of charge separation processes. Our experimental data, derived from accurate IQE measurements on homojunction solar cells, is in good agreement with the predicted error-function dependence on photon energy. From this, we show that disorder in eight common organic semiconductors is somewhat larger than previously thought, a finding that may influence how the performance of devices made of these materials is interpreted. More broadly, reliable measurements of energetic disorder are vital if we are to understand charge generation and transport and facilitate the design of more efficient organic electronics.

Supporting Information

Details of materials used in this work with chemical structures; absorption spectra; EQE measurements and reflection spectra; IQE calculation details; detailed simulation results with sensitivity analysis; simulated and experimental data in the presence of an electric field.

Acknowledgements

Author contributions

S.N.H. performed the simulations; N.Z. carried out the device fabrication and characterisation; P.M., A.A., and I.K. oversaw the project; and all authors interpreted the results and wrote the manuscript.

Competing financial interests

The authors declare no competing financial interests.

References

(1) Lee, E. M. Y.; Tisdale, W. A.; Willard, A. P. Can Disorder Enhance Incoherent Exciton Diffusion? *J. Phys. Chem. B* **2015**, *119*, 9501–9509.

(2) Bässler, H.; Köhler, A. *Electronic Processes in Organic Semiconductors*; Wiley-VCH, 2015.

(3) Bässler, H. Charge Transport in Disordered Organic Photoconductors. *Phys. Status Solidi B* **1993**, *175*, 15–56.

(4) Noriega, R.; Rivnay, J.; Vandewal, K.; Koch, F. P. V.; Stingelin, N.; Smith, P.; Toney, M. F.; Salleo, A. A General Relationship Between Disorder, Aggregation and Charge Transport in Conjugated Polymers. *Nat. Mater.* **2013**, *12*, 1038–1044.

(5) Oelerich, J. O.; Huemmer, D.; Baranovskii, S. D. How to Find out the Density of States in Disordered Organic Semiconductors. *Phys. Rev. Lett.* **2012**, *108*, 1–5.

(6) Coropceanu, V.; Cornil, J.; da Silva, D. A.; Olivier, Y.; Silbey, R.; Brédas, J.-L. Charge Transport in Organic Semiconductors. *Chem. Rev.* **2007**, *107*, 926–952.

(7) Clarke, T. M.; Durrant, J. R. Charge Photogeneration in Organic Solar Cells. *Chem. Rev.* **2010**, *110*, 6736–6767.

(8) Hood, S. N.; Kassal, I. Entropy and Disorder Enable Charge Separation in Organic Solar Cells. *J. Phys. Chem. Lett.* **2016**, *7*, 4495–4500.

(9) Shi, L.; Lee, C. K.; Willard, A. P. The Enhancement of Interfacial Exciton Dissociation by Energetic Disorder Is a Nonequilibrium Effect. *ACS Central Science* **2017**, *3*, 1262–1270.

(10) Groves, C.; Marsh, R. A.; Greenham, N. C. Monte Carlo Modeling of Geminate Recombination in Polymer-Polymer Photovoltaic Devices. *J. Chem. Phys.* **2008**, *129*, 1–7.

(11) Blakesley, J. C.; Neher, D. Relationship Between Energetic Disorder and Open-Circuit Voltage in Bulk Heterojunction Organic Solar Cells. *Phys. Rev. B* **2011**, *84*, 075210.

(12) Heumueller, T.; Burke, T. M.; Mateker, W. R.; Sachs-Quintana, I. T.; Vandewal, K.; Brabec, C. J.; McGehee, M. D. Disorder-Induced Open-Circuit Voltage Losses in Organic Solar Cells During Photoinduced Burn-In. *Adv. Energy Mater.* **2015**, *5*, 1500111.

(13) Urbach, F. The Long-Wavelength Edge of Photographic Sensitivity and of the Electronic Absorption of Solids. *Phys. Rev.* **1953**, *92*, 1324.

(14) Sa-Yakanit, V.; Glyde, H. R. Urbach Tails and Disorder. *Comments Condens. Matter Phys.* **1987**, *13*, 35–48.

(15) Street, R. A. *Hydrogenated Amorphous Silicon*; Cambridge University Press: Cambridge, 1991.

(16) Deibel, C.; Mack, D.; Gorenflot, J.; Schöll, A.; Krause, S.; Reinert, F.; Rauh, D.; Dyakonov, V. Energetics of Excited States in the Conjugated Polymer Poly(3-hexylthiophene). *Phys. Rev. B* **2010**, *81*, 1–5.

(17) Kronemeijer, A. J.; Pecunia, V.; Venkateshvaran, D.; Nikolka, M.; Sadhanala, A.; Moriarty, J.; Szumilo, M.; Sirringhaus, H. Two-Dimensional Carrier Distribution in Top-Gate Polymer Field-Effect Transistors: Correlation Between Width of Density of Localized States and Urbach Energy. *Adv. Mater.* **2014**, *26*, 728–733.

(18) Samiee, M.; Joshi, P.; Aidarkhanov, D.; Dalal, V. Measurement of Defect Densities and Urbach Energies of Tail States in PTB7 Solar Cells. *Appl. Phys. Lett.* **2014**, *105*, 133511.

(19) Venkateshvaran, D.; Nikolka, M.; Sadhanala, A.; Lemaur, V.; Zelazny, M.; Kepa, M.; Hurhangee, M.; Kronemeijer, A. J.; Pecunia, V.; Nasrallah, I. et al. Approaching Disorder-Free Transport in High-Mobility Conjugated Polymers. *Nature* **2014**, *515*, 384–388.

(20) Gong, W.; Faist, M. A.; Ekins-Daukes, N. J.; Xu, Z.; Bradley, D. D.; Nelson, J.; Kirchartz, T. Influence of Energetic Disorder on Electroluminescence Emission in Polymer: Fullerene Solar Cells. *Phys. Rev. B* **2012**, *86*, 1–9.

(21) Zhao, B.; Abdi-Jalebi, M.; Tabachnyk, M.; Glass, H.; Kamboj, V. S.; Nie, W.; Pearson, A. J.; Puttisong, Y.; Gödel, K. C.; Beere, H. E. et al. High Open-Circuit Voltages in Tin-Rich Low-Bandgap Perovskite-Based Planar Heterojunction Photovoltaics. *Adv. Mater.* **2017**, *29*, 1604744.

(22) Jain, N.; Chandrasekaran, N.; Sadhanala, A.; Friend, R.; McNeill, C. R.; Kabra, D. Interfacial Disorder in Efficient Polymer Solar Cells: Impact of Donor Molecular Structure and Solvent Additive. *J. Mater. Chem. A* **2017**, *5*, 24749–24757.

(23) Borsenberger, P. M.; Pautmeier, L.; Bässler, H. Charge Transport in Disordered Molecular Solids. *J. Chem. Phys.* **1991**, *94*, 5447–5454.

(24) Meskers, S. C. J.; Hübner, J.; Oestreich, M.; Bässler, H. Broadband Ultrafast Photoluminescence Spectroscopy Resolves Charge Photogeneration via Delocalized Hot Ex-

citons in Polymer:Fullerene Photovoltaic Blends. *J. Phys. Chem. B* **2001**, *105*, 9139–9149.

(25) Offermans, T.; Meskers, S. C. J.; Janssen, R. A. J. Charge Recombination in a Poly(Para-Phenylene Vinylene)-Fullerene Derivative Composite Film Studied by Transient, Nonresonant, Hole-Burning Spectroscopy. *J. Chem. Phys.* **2003**, *119*, 10924–10929.

(26) Mihailetchi, V. D.; Van Duren, J. K. J.; Blom, P. W. M.; Hummelen, J. C.; Janssen, R. A. J.; Kroon, J. M.; Rispens, M. T.; Verhees, W. J. H.; Wienk, M. M. Electron Transport in a Methanofullerene. *Adv. Funct. Mater.* **2003**, *13*, 43–46.

(27) Peumans, P.; Forrest, S. R. Separation of Geminate Charge-Pairs at Donor–Acceptor Interfaces in Disordered Solids. *Chem. Phys. Lett.* **2004**, *398*, 27–31.

(28) Marsh, R. A.; Groves, C.; Greenham, N. C. A Microscopic Model for the Behavior of Nanostructured Organic Photovoltaic Devices. *J. Appl. Phys.* **2007**, *101*, 083509.

(29) Rörich, I.; Mikhnenko, O. V.; Gehrig, D.; Blom, P. W. M.; Crăciun, N. I. Influence of Energetic Disorder on Exciton Lifetime and Photoluminescence Efficiency in Conjugated Polymers. *J. Phys. Chem. B* **2017**, *8*, 1405–1412.

(30) Gali, S. M.; D'Avino, G.; Aurel, P.; Han, G.; Yi, Y.; Papadopoulos, T. A.; Coropceanu, V.; Brédas, J. L.; Hadziioannou, G.; Zannoni, C. et al. Energetic Fluctuations in Amorphous Semiconducting Polymers: Impact on Charge-Carrier Mobility. *J. Chem. Phys.* **2017**, *147*.

(31) Lange, I.; Blakesley, J. C.; Frisch, J.; Vollmer, A.; Koch, N.; Neher, D. Band Bending in Conjugated Polymer Layers. *Phys. Rev. Lett.* **2011**, *106*, 216402.

(32) Karki, A.; Wetzelaer, G.-J. A. H.; Reddy, G. N. M.; Nádaždy, V.; Seifrid, M.; Schauer, F.; Bazan, G. C.; Chmelka, B. F.; Blom, P. W. M.; Nguyen, T.-Q. Unifying

Energetic Disorder from Charge Transport and Band Bending in Organic Semiconductors. *Adv. Funct. Mater.* **2019**, *29*, 1901109.

(33) Blakesley, J. C.; Greenham, N. C. Charge Transfer at Polymer-Electrode Interfaces: The Effect of Energetic Disorder and Thermal Injection on Band Bending and Open-Circuit Voltage. *J. Appl. Phys.* **2009**, *106*, 034507.

(34) Tal, O.; Rosenwaks, Y.; Preezant, Y.; Tessler, N.; Chan, C. K.; Kahn, A. Direct Determination of the Hole Density of States in Undoped and Doped Amorphous Organic Films with High Lateral Resolution. *Phys. Rev. Lett.* **2005**, *95*, 256405.

(35) Hu, Y.; Jiang, L.; Chen, Q.; Guo, J.; Chen, Z. Direct Observation of the Dipole-Induced Energetic Disorder in Rubrene Single-Crystal Transistors by Scanning Kelvin Probe Microscopy. *J. Phys. Chem. Lett.* **2018**, *9*, 2869–2873.

(36) Young, R. H. Dipolar Lattice Model of Disorder in Random Media Analytical Evaluation of the Gaussian Disorder Model. *Philos. Mag. B* **1995**, *72*, 435–457.

(37) Li, J.; Zhao, Y.; Tan, H. S.; Guo, Y.; Di, C. A.; Yu, G.; Liu, Y.; Lin, M.; Lim, S. H.; Zhou, Y. et al. A Stable Solution-Processed Polymer Semiconductor with Record High-Mobility for Printed Transistors. *Sci. Rep.* **2012**, *2*, 1–9.

(38) Armin, A.; Velusamy, M.; Wolfer, P.; Zhang, Y.; Burn, P. L.; Meredith, P.; Pivrikas, A. Quantum Efficiency of Organic Solar Cells: Electro-Optical Cavity Considerations. *ACS Photonics* **2014**, *1*, 173–181.

(39) Marcus, R. A. Electron Transfer Reactions in Chemistry. Theory and Experiment. *Rev. Mod. Phys.* **1993**, *65*, 599.

(40) Miller, A.; Abrahams, E. Impurity Conduction at Low Concentrations. *Phys. Rev.* **1960**, *120*, 745–755.

(41) Vandewal, K.; Tvingstedt, K.; Gadisa, A.; Inganäs, O.; Manca, J. V. Relating the Open-Circuit Voltage to Interface Molecular Properties of Donor:Acceptor Bulk Heterojunction Solar Cells. *Phys. Rev. B* **2010**, *81*, 125204.

(42) Jankowiak, R.; Rockwitz, K. D.; Bässler, H. Adsorption Spectroscopy of Amorphous Tetracene. *J. Phys. Chem.* **1983**, *87*, 552–557.

(43) Hoffmann, S. T.; Bässler, H.; Köhler, A. What Determines Inhomogeneous Broadening of Electronic Transitions in Conjugated Polymers? *J. Phys. Chem. B* **2010**, *114*, 17037–17048.

(44) Mozer, A. J.; Sariciftci, N. S. Negative Electric Field Dependence of Charge Carrier Drift Mobility in Conjugated, Semiconducting Polymers. *Chem. Phys. Lett.* **2004**, *389*, 438 – 442.

(45) Ballantyne, A. M.; Chen, L.; Dane, J.; Hammant, T.; Braun, F. M.; Heeney, M.; Duffy, W.; McCulloch, I.; Bradley, D. D. C.; Nelson, J. The Effect of Poly(3-hexylthiophene) Molecular Weight on Charge Transport and the Performance of Polymer:Fullerene Solar Cells. *Adv. Funct. Mater.* **2008**, *18*, 2373–2380.

(46) Inigo, A. R.; Chiu, H.-C.; Fann, W.; Huang, Y.-S.; Jeng, U.-S.; Lin, T.-L.; Hsu, C.-H.; Peng, K.-Y.; Chen, S.-A. Disorder Controlled Hole Transport in MEH-PPV. *Phys. Rev. B* **2004**, *69*, 075201.

(47) Melianas, A.; Etzold, F.; Savenije, T. J.; Laquai, F.; Inganäs, O.; Kemerink, M. Photo-Generated Carriers Lose Energy During Extraction from Polymer-Fullerene Solar Cells. *Nat. Commun.* **2015**, *6*, 8778.

(48) Roland, S.; Kniepert, J.; Love, J. A.; Negi, V.; Liu, F.; Bobbert, P.; Melianas, A.; Kemerink, M.; Hofacker, A.; Neher, D. Equilibrated Charge Carrier Populations Govern Steady-State Nongeminate Recombination in Disordered Organic Solar Cells. *J. Phys. Chem. Lett.* **2019**, *10*, 1374–1381.

(49) Burke, T. M.; Sweetnam, S.; Vandewal, K.; McGehee, M. D. Beyond Langevin Recombination: How Equilibrium Between Free Carriers and Charge Transfer States Determines the Open-Circuit Voltage of Organic Solar Cells. *Adv. Energy Mater.* **2015**, *5*, 1500123.

(50) Tummala, N. R.; Zheng, Z.; Aziz, S. G.; Coropceanu, V.; Brédas, J.-L. Static and Dynamic Energetic Disorders in the C_{60}, $PC_{61}BM$, C_{70}, and $PC_{71}BM$ Fullerenes. *J. Phys. Chem. Lett.* **2015**, *6*, 3657–3662.